Low-Level Inversions over the Tropical Pacific—Thermodynamic Structure of the Boundary Layer and the Above-Inversion Moisture Structure

KEVIN A. KLOESEL AND BRUCE A. ALBRECHT

The Pennsylvania State University, Department of Meteorology, University Park, Pennsylvania

(Manuscript received 27 August 1987, in final form 14 July 1988)

ABSTRACT

The structure of the boundary layer over a broad region of the equatorial Pacific is studied using dropwindsonde measurements made in January, February, May, and June of 1979. Low-level inversions of sufficient strength to inhibit deep convection are found to be present in more than 50% of the soundings. These inversions appear to play a critical role in regulating convective activity over the central and eastern Pacific. The tops of the inversions have an average pressure level of approximately 800 mb and show little latitudinal or longitudinal variation. The majority of the inversion soundings (approximately 70%) have a reversal in the mixing ratio profile (q-reversal) above the inversion that appears as a dry layer at the top of the inversion layer capped by a relatively moist layer. This moist layer is on the average 2 g kg^{-1} more moist than the corresponding soundings that have no q-reversal. No systematic regional or temporal variations in the frequency of occurrence of the q-reversal or the structure of the boundary layer associated with this feature were observed. In previous studies it was suggested that the q-reversal could be formed by nearby convection that is penetrating to higher levels, moistening those levels, and producing downdrafts that spread out at the top of the inversion as a dry layer. Differences between the thermodynamic structure of soundings with and that without the q-reversal support this idea. It is suggested that relatively dry layers may form above inversions of all types and heights in areas where there is nearby convection and associated downdrafts.

1. Introduction

The atmospheric boundary layer over tropical and subtropical oceans plays a critical role in regulating surface energy and moisture fluxes and in controlling the convective transfer of energy and moisture to the free atmosphere. Consequently, many field studies in the tropics and subtropics have attempted to define and explain the structure of the convective boundary layer. Data collected during the Barbados Oceanic and Meteorological Experiment (BOMEX), 1969 (Holland and Rasmusson 1973) and the Atlantic Trade-Wind Experiment (ATEX) 1969 (Augstein et al. 1973) focused on the structure of the boundary layer during suppressed convective conditions. Data collected during the GARP Atlantic Tropical Experiment (GATE), 1974 were used to describe the structure of the subcloud layer and the lower part of the cloud layer in association with deep convection, and during the recovery of the boundary layer following disturbed convective conditions (Houze 1977; Zipser 1977; Fitzjarrald and Garstang 1981). Measurements made from aircraft have also been used to study the turbulent structure of the subcloud layer (LeMone and Pennell 1976; Nicholls and LeMone 1980) and the interaction between the subcloud and the cloud layer.

Corresponding author address: Kevin A. Kloesel, Dept. of Meteorology, 503 Walker Building, The Pennsylvania State University, University Park, PA 16802.

Radiosonde data have been used to study the structure of the atmosphere over the tropical Pacific (Reed and Recker 1971; Yanai et al. 1973). The data used in these studies were of insufficient vertical resolution to make detailed studies of the structure of the boundary layer.

Data from dropwindsondes launched over the tropical Pacific during the First GARP Global Experiment (FGGE) during January and February of 1979 (during Special Observing Period (SOP-I) were used to study gross features of the boundary layer over the central Pacific (Firestone and Albrecht 1986; Betts and Albrecht 1987). These FGGE observations are of particular interest since they were made over a relatively broad region of the tropical Pacific—a region where the boundary layer may play a critical role in regulating convective activity and air–sea interactions on a variety of time and space scales.

In this paper we extend the FGGE studies of Firestone and Albrecht (1986, hereafter referred to as FA86) and Betts and Albrecht (1987, hereafter referred to as BA87) to include dropwindsonde data collected during April and May of 1979 (during SOP II) and soundings obtained over the eastern Pacific during both SOP I and II. In FA86 it is argued that low-level inversions are important for regulating convective activity near the equator. We use the complete FGGE Pacific dropwindsonde dataset to compile comprehensive statistics on the occurrence of low-level inversions that cap a shallow cloud layer between 5°S and 15°N from

90°W to 170°E during January, February, May and June of 1979, and to describe the structure of the boundary layer for this period. Our definition of the boundary layer is that used by Augstein et al. (1974), Stull (1988) and others. It is that part of the troposphere that is directly coupled to surface processes and includes fair-weather cumulus clouds and stratocumulus clouds.

A major focus of modeling and theoretical work on the marine boundary layer for suppressed convective conditions has been on how convective, radiative, and large-scale processes maintain the thermodynamic structure of the boundary layer associated with shallow cumulus clouds (Betts 1973; Albrecht et al. 1979). Relatively little consideration, however, has been given to the thermodynamic structure above the inversion. It has generally been assumed that the large-scale and the radiative processes at this level would be adequately resolved by an appropriate large-scale model. Observations, however, indicate that under many circumstances the moisture structure above the inversion is relatively complicated. In BA87, a subset of the dropwindsonde soundings obtained during SOP I of FGGE showed a well-defined reversal of the vertical gradient of mixing ratio (q) (hereafter referred to as the q-reversal or "QR") above the inversion. This structure was highlighted by conserved parameter plots (Betts 1985). The stratification gives the appearance of a relatively dry layer just above the inversion. An example of this stratification is shown in Fig. 1 for a sounding obtained on 17 May 1979 at 6.12°N, 103°W, 1300 LST. The dry layer from 860 to 820 mb is associated with a stable layer at about 850 mb that caps the cloud layer. A moist intrusion occurs above the stable layer (from 820 to 750 mb) and there is a weak stable layer at the top of this moist layer. If in this case the top of the boundary layer is defined at 850 mb, one is immediately faced with the difficulty of defining a simple moisture structure above the inversion. Thus, the QR has important implications concerning the appropriate upper boundary to use for the representation of the boundary layer in a large-scale model.

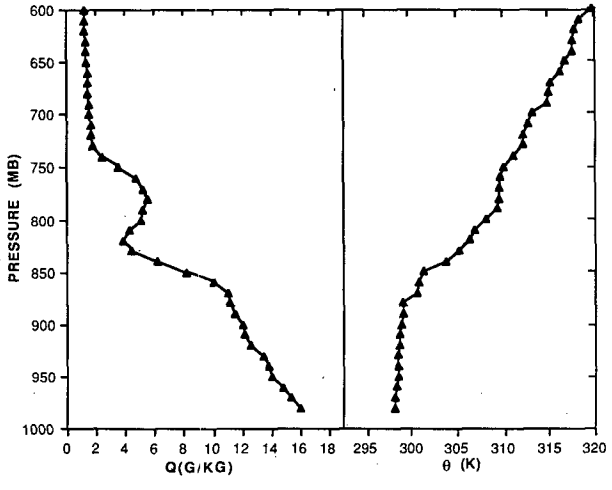

FIG. 1. Mixing ratio and potential temperature profiles for a FGGE equatorial Pacific sounding (17 May 1979 at 6.12°N, 103°W, 1300 LST).

Since the BA87 study was based on a limited number of soundings (116 total), we attempt to establish the frequency of occurrence of the QR for a broad region of the Pacific by including SOP II soundings and soundings from the eastern Pacific. In addition, we compare the mean thermodynamic structure for soundings with and without the QR and consider possible mechanisms for the formation and maintenance of the above-inversion structure. Specific consideration is given to the role that penetrating convection may play in forming the QR structure.

The dataset is described and the possible contributions of instrument error to the QR are discussed in section 2. In section 3 we describe the scheme used to classify the soundings obtained from the dropwindsondes and present statistics on these classifications and on the low-level inversions in this dataset. In section 4 statistics on the occurrence of the QR and the mean thermodynamic structure associated with this feature are discussed. A discussion of how the QR may be formed is presented in section 5.

2. Description of data and error analysis

Dropwindsondes were launched over the equatorial Pacific Ocean (170°E to 90°W) from 15 January 1979 to 20 February 1979 during SOP I, and 10 May 1979 to 8 June 1979 during SOP II and resulted in the collection of over two thousand soundings (Fleming et al. 1979a,b). The dropwindsondes were launched from United States Air Force C-141 aircraft during flights originating from Hickam Field in Hawaii, and Acapulco International Airport in Mexico. Due to problems in obtaining operating rights to Acapulco, several missions in SOP I were flown from Howard Air Force Base in the Panama Canal Zone, and Norton Air Force Base in California. Usually, two flights were flown daily along the flight paths shown in Fig. 2 (Tiernan 1981). The flight patterns were altered by one to two degrees latitude to avoid flying through areas of intense convection and areas where FGGE ships were collecting upper air data (Julian 1982). The dropwindsondes were launched from an altitude of approximately 13 kilometers at intervals of approximately 350 kilometers along the flight path. The sondes were used to obtain temperature, relative humidity, wind speed, and wind direction profiles as a function of pressure. Temperature was sensed by a bead thermistor and humidity was sensed by a carbon hygristor similar to that used in standard U.S. radiosondes, but modified for a faster response (Scribner and Smalley 1981).

For each sounding, data were transmitted from the sonde to the aircraft at ten second intervals (approxi-

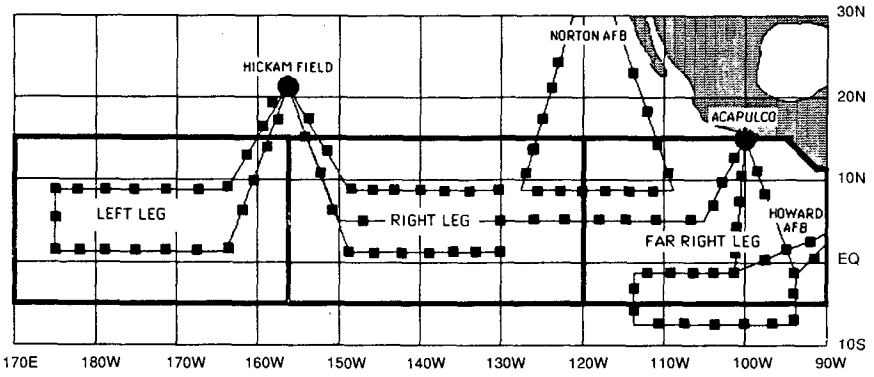

FIG. 2. Mean dropwindsonde flight paths during FGGE and the boundaries for the regional categories (after Tiernan 1981).

mately 4 mb intervals since the fall speed was approximately 25 millibars per minute). The data reduction follows that described by FA86. A 1–2–1 smoother (50% of the raw value at the level of interest + 25% of the raw value at the next level above + 25% of the raw value at the next level below) was applied to the ten second temperature and the dewpoint depression values (obtained via raw relative humidity). The smoothed data were then interpolated to 10 mb intervals and were used to compute mixing ratio (q), potential temperature (θ), equivalent potential temperature (θ_e), and saturation equivalent potential temperature (θ_{es}). The soundings were then examined subjectively to eliminate those soundings containing deep superadiabatic layers (30 mb or greater), anomalously high temperatures, and suspect relative humidity profiles.

Since the QR is often described as "spurious" and "erroneous" (e.g., Lilly 1968), it becomes necessary to assess its validity in the FGGE soundings. Using four randomly selected soundings (with the QR) from the FGGE dataset, the possibility of the QR being caused by sensor error was examined. Since the mixing ratios used in this study were calculated using temperature and relative humidity, errors in either of these quantities could alter the q profile. Differences between the real soundings and the modified soundings were examined to determine whether the modifications of relative humidity and temperature needed to remove the QR lie within the error specifications of the sensors.

Smoothing the q profile for the four sample soundings required that the relative humidity be increased by an absolute value of 8%–15% in the region of the QR; if we attempt to explain the QR by errors in temperature, a 3°–9°C temperature difference would be required. These values exceed the expected accuracy of 1°C for the temperature sensor and 5% for the relative humidity sensor. Furthermore, the precision, which is the relevant factor for vertical gradients, will be greater than the accuracy. A comparison of dropwindsonde soundings made in the vicinity of rawindsonde stations (Julian 1982) indicated no differences greater than those due to the expected sensor error variances. Since the QR occurs in a region where the temperature does not change as rapidly as it does in the inversion layer, and since we found that the QR occurs most frequently in regions away from deep convection, it is difficult to explain the QR as an artifact of instrument response time or of a wetting of either the humidity or the temperature sensor. Thus, it is unlikely that the QR observed in the FGGE tropical soundings is due to instrument errors.

3. Classification of soundings and inversion statistics

The soundings were separated into regional groups to evaluate the longitudinal variations in the sounding statistics and the structure of the boundary layer. Only soundings between 15°N and 5°S were used in the analysis. The longitudinal separations are illustrated in Fig. 2 and are 170°E to 157°W for LEFT LEG (LL), 157° to 120°W for RIGHT LEG (RL), and 120° to 90°W for the FAR RIGHT LEG (FRL).

The soundings in each regional group were classified on the basis of low-level stability. These classifications were intended to characterize differences in the thermodynamic structure of the boundary layer associated with deep convection, shallow convection, and conditions where both deep and shallow convection may be suppressed. The classifications were based on θ_e and θ_{es} profiles for each sounding. Betts (1974) classified soundings obtained during the Venezuelan International Meteorological and Hydrological Experiment on the basis of area rainfall rates and studied the θ_e and θ_{es} profiles for these classifications. Here we use the θ_e and θ_{es} profiles to infer the convective activity. Idealized profiles that illustrate this classification are shown in Fig. 3. For each sounding we considered the ascent of a nonentraining air parcel from 980 mb. At levels above the LCL of this parcel, the difference between the constant θ_e path of the parcel and the θ_{es} of the sounding is proportional to the temperature difference between

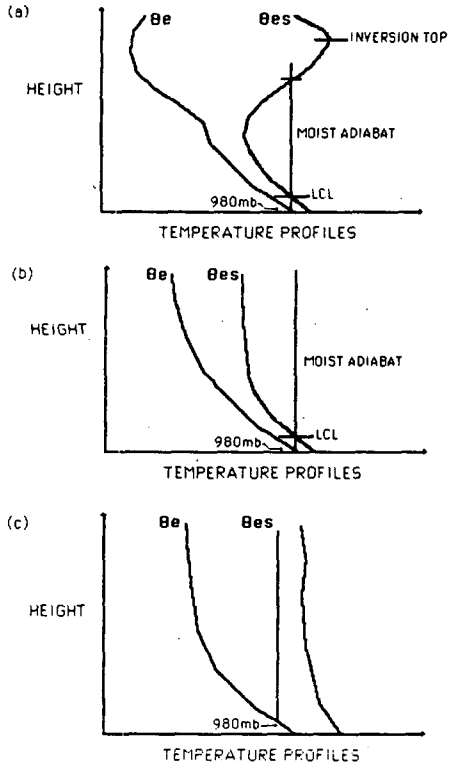

FIG. 3. Idealized thermodynamic structure for (a) the Inversion group, (b) the High Theta E group, and (c) the Low Theta E group.

the parcel and its environment. If θ_e of the 980 mb parcel path (θ_e') was greater than θ_{es} above the LCL, but intersected the θ_{es} profile at a pressure greater than 600 mb, the sounding was classified as an *Inversion* sounding (Fig. 3a). Satellite images indicate that these soundings occur in regions of fair-weather cumulus or stratus clouds. If a 980 mb parcel was positively buoyant ($\theta_e' > \theta_{es}$) above the LCL to at least the 600 mb level, the sounding was classified as *High Theta E* (Fig. 3b). These unstable soundings are generally associated with regions of deep convection. If the low-level parcel was negatively buoyant ($\theta_e' \leqslant \theta_{es}$) to the 600 mb level, the sounding was classified as *Low Theta E* (Fig. 3c). Although entrainment and virtual temperature effects should be used to make quantitative estimates of buoyancy, the simple scheme we use provides an unambiguous classification of almost all of the soundings that were screened in the FGGE dropwindsonde set.

Of the soundings that remained after the subjective screening for data quality and the regional grouping of the soundings, only those obtained between 0600 and 1400 LST were included in the analysis. A total of 93% of the soundings were made during these hours and 1242 soundings remained after the various screening procedures. The number and percentage of soundings in each thermodynamic category is given in Table 1. The percentage of soundings in each region for each classification is shown in Table 2. Although 62% of all the soundings were classified as stable (Inversion or Low Theta E) these statistics may be biased in favor of the stable sounding since the aircraft that deployed the dropwindsondes avoided the areas of deepest convection. The left region had the lowest ratio between stable and unstable soundings (1.0 during SOP I and 0.8 during SOP II). The FA86 study was based on SOP I soundings in LL and RL. The BA87 study was based on SOP I Inversion soundings in LL and RL.

The sea-surface temperatures (SSTs) for these categories of soundings were estimated using the Comprehensive Ocean Atmosphere Data Set (COADS) data from January, February, May and June 1979. These data were plotted and subjectively smoothed. The smoothed fields were represented on a grid and the SSTs were obtained by interpolating to the latitude and longitude of each sounding. The average temperature for each region was then obtained for the different thermodynamic classifications. The soundings for all thermodynamic classifications in the LL had an average SST of about 28°C during both SOP I and SOP II. The SST for RL was approximately 27°C, and the FRL SST was about 26°C in SOP I and 27°C in SOP II. The SSTs calculated for ensembles of soundings in each of the thermodynamic classifications varied little within a given region.

In FA86, the GOES West IR satellite images were used to classify the SOP I soundings in regions LL and RL as either disturbed (unstable) or undisturbed (stable). Soundings in the vicinity of high clouds as indicated by regions of low outgoing IR radiation were classified as disturbed. Those away from regions of deep convection were classified as stable or undisturbed. In the FA86 classification, 52% of the soundings were classified as stable, which is 10% lower than the 62% obtained using the thermodynamic classification described here. Since the FA86 classification was based on satellite images, their disturbed classification could include soundings with inversions that were in regions under upper-level clouds but away from deep convection. The SOP I convective classification statistics for the FRL are similar to those of the RL. In our study of SOP II soundings, 54% of the soundings have a low-level inversion of sufficient strength to significantly inhibit deep convection. For both SOP I and SOP II, 53% of the soundings have a low-level inversion. A

TABLE 1. The number and percentage of FGGE soundings in the different thermodynamic classifications, and by Special Observing Period, SOP I and SOP II.

	SOP I	SOP II	Total
Inversion	400 (51.7%)	256 (54.6%)	656 (52.8%)
High Theta E	285 (36.9%)	165 (35.2%)	450 (36.2%)
Low Theta E	88 (11.4%)	48 (10.2%)	136 (11.0%)
Total	773 (100%)	469 (100%)	1242 (100%)

TABLE 2. Breakdown of soundings by thermodynamic classification, region, and SOP.

	Inversion		High Theta E		Low Theta E		Total number of soundings	
	SOP I	SOP II	SOP I	SOP II	SOP I	SOP II	SOP I	SOP II
Left leg	42%	39%	50%	55%	8%	6%	288	152
Right leg	58%	65%	30%	25%	23%	10%	299	171
Far right leg	56%	59%	28%	26%	16%	15%	186	146

slightly lower percentage of Inversion soundings was observed over the central Pacific than over the eastern Pacific.

The results from this study are consistent with the limited study of FA86 and indicate that low-level inversions play a key role in regulating convection over a broad region of the eastern and central Pacific during January, February, May and June of 1979. Ramage et al. (1981) came to a similar conclusion using data collected from aircraft transects between Hawaii and Tahiti.

The dropwindsonde data were used to describe the regional and seasonal variability in the thermodynamic structure associated with the Inversion soundings. The inversion top for each Inversion sounding was determined by the location of the maximum in the θ_{es} profile, and the minimum of the θ_e profile (see BA87). Soundings containing multiple inversions were eliminated from this classification to avoid the possibility of having one sounding appear in two inversion-top groups. This eliminated 81 soundings (66 with a QR) from SOP I, and 41 soundings (29 with a QR) from SOP II. Figure 4 shows the distribution of inversion heights for SOP I and SOP II. The inversion heights over the entire central and eastern Pacific over two different time periods (Jan–Feb 1979 and May–Jun 1979), are normally distributed with a peak in the distribution occurring with inversion tops located near 800 mb.

The variation of inversion heights with latitude and longitude was evaluated by averaging heights (pressure levels) in 5° by 5° areas. The average inversion height was then calculated for areas that contained at least four soundings. The results in Fig. 5 show that for both SOP I and SOP II there is little variation in the average height of the inversion over the entire central and eastern Pacific. The average inversion top pressure is about 810 mb in all regions. This relatively constant inversion height is consistent with the north–south potential temperature cross section presented in FA86 and by the aircraft observations described by Ramage et al. (1981). It is clear that the typical depiction of the trade inversion increasing in height as air moves equatorward in the trades (e.g. Riehl et al. 1951) does not apply between 15°N and the equator over the Pacific. Although the frequency of inversion occurrence decreases equatorward, the height of the inversions is relatively constant despite the presence of large-scale convergence and upward motion in this region (FA86). Apparently the subsidence in the regions surrounding the deep convection is of sufficient strength to maintain relatively low inversions. Thus, although the frequency of occurrence of inversions in the LL is less than in the RL and FRL regions, the inversion height is about the same at all longitudes. Furthermore, it is possible that as the depth of the cloud layer increases, some of the clouds will precipitate. This removal of water decreases the ability of the clouds to deepen the boundary layer by the evaporation of moisture at the top of the cloud layer and stabilizes the boundary layer. Thus, the convective coupling between the surface and the top of the boundary layer is weakened.

Our extended analysis shows that in all regions and for both SOP I and SOP II, higher inversions are often

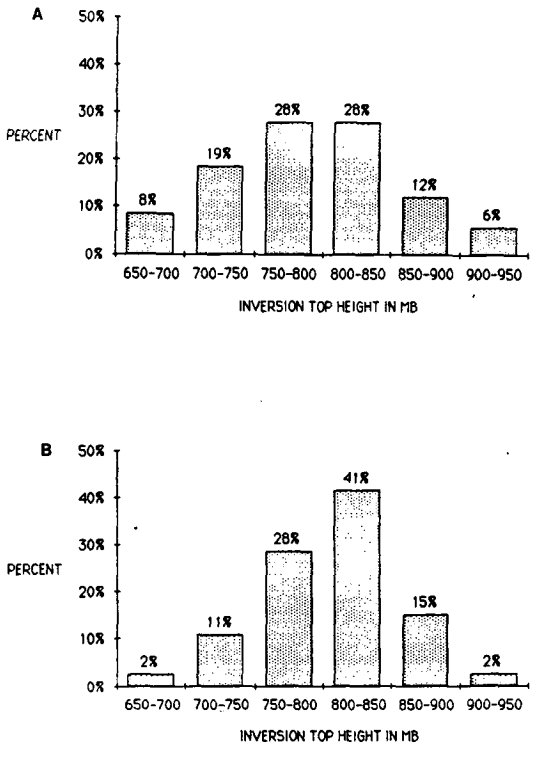

FIG. 4. Percent of SOP I Inversion soundings in each inversion height category for (a) SOP I and (b) SOP II.

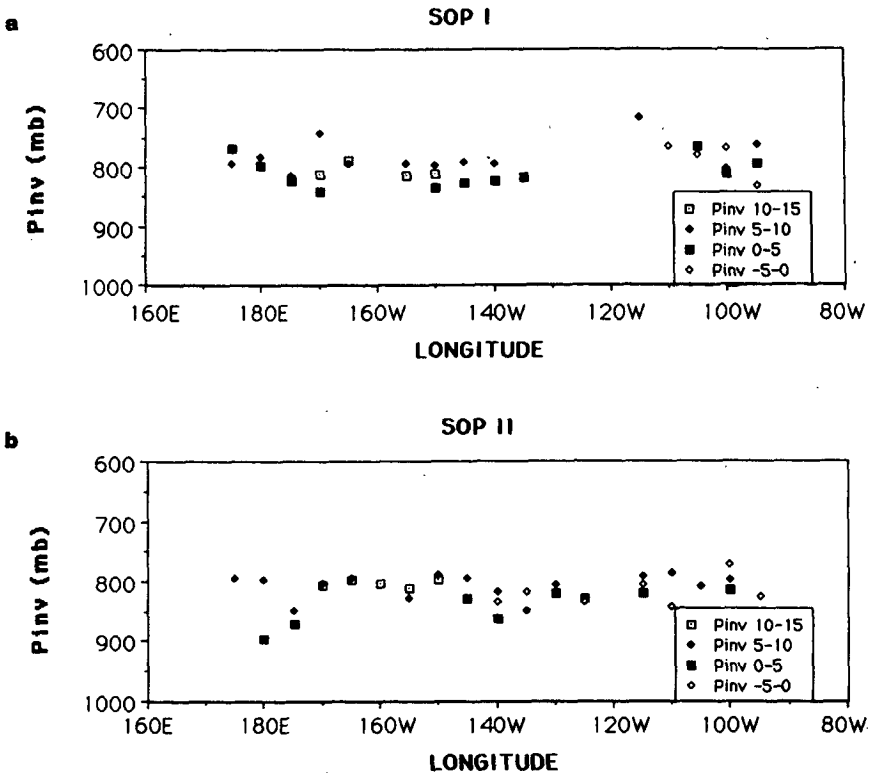

FIG. 5. Average inversion heights for (a) SOP I and (b) SOP II. The symbols indicate the latitude ranges as indicated in the legend.

associated with a double inversion structure where the lower inversion is near 850 mb and the upper inversion is near 750 mb. This further supports the assertions of BA87 that at times there may be two distinct cloud populations in regions of convectively suppressed conditions. Furthermore, as discussed in BA87, the deeper clouds may be responsible for maintaining the QR structure above lower cloud layers.

4. QR statistics and mean profiles

The soundings were subjectively examined for evidence of a QR structure. For Inversion soundings a QR was defined as an increase in the mixing ratio of at least 1 g kg^{-1} above the inversion top followed by the normal decrease with height. We eliminated the possible bias of a single bad point by requiring that the increase occur over a 20 mb layer. In addition, the QR structure was evident in a number of the High Theta E and the Low Theta E data soundings. In these soundings only QR features that occurred between 900 and 750 mb were considered. The percentage of soundings with the QR for the various subsets is shown in Table 3. In all but two subsets the QR occurred in more than 50% percent of the soundings. The data in Table 3 indicate that:

(i) The QR was observed in approximately 68% of all the soundings studied.

(ii) The QR occurred more frequently in SOP I than in SOP II (72% to 63%).

(iii) Soundings with inversions were more likely to have the QR than those without, and the stable soundings (Inversion and Low Theta E) were more likely to have a QR (72%) than the unstable soundings (62%).

(iv) The RL region has slightly more QR soundings than the other two regions.

The location of the Inversion soundings with QRs relative to those with no QR (NQR) is shown in Fig.

TABLE 3. Percentage of soundings in each thermodynamic category, region, and SOP containing the q-reversal profile.

	Region LL	Region RL	Region FRL	Total
		SOP I		
Inversion	65.6	85.5	74.3	76.5
High Theta E	58.0	73.3	69.0	64.9
Low Theta E	56.5	69.4	82.8	70.5
Total	61.1	80.0	74.2	71.5
		SOP II		
Inversion	67.8	67.6	62.8	67.0
High Theta E	57.1	69.8	42.1	57.0
Low Theta E	44.4	88.0	59.0	66.6
Total	60.5	70.2	56.8	62.7

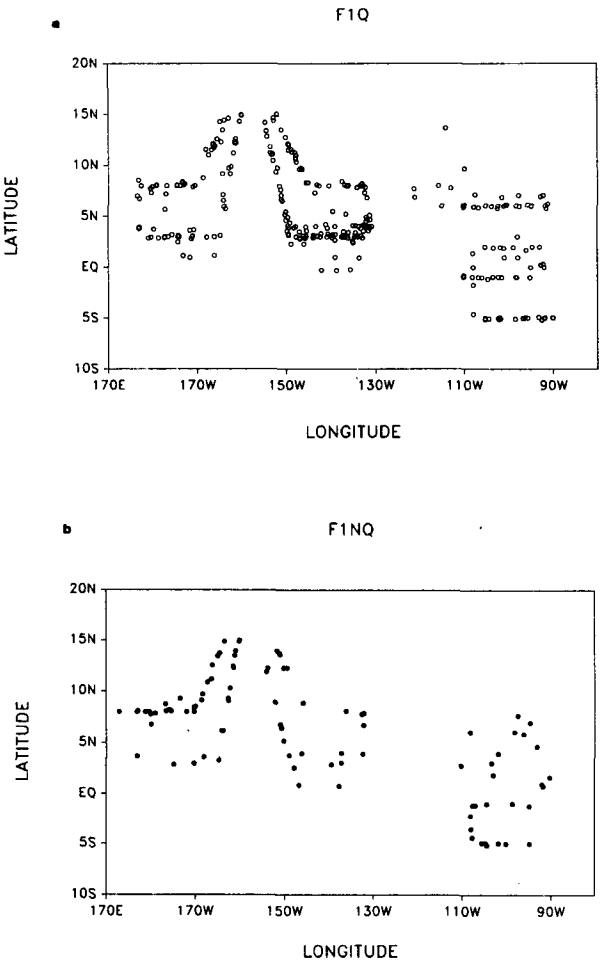

FIG. 6. Location of SOP I soundings (a) with QR and (b) without QR.

6 for SOP I and Fig. 7 for SOP II. The distribution indicates no preferred location for the QR soundings. Thus it would be difficult to explain the QR as a consequence of differential advection, unless such conditions exist over the entire eastern and central Pacific during the two periods studied.

The average thermodynamic structure for the Inversion soundings with the QR show little seasonal or longitudinal variations. This is illustrated in Fig. 8 where profiles of θ_e and θ_{es} obtained for soundings in Region LL, SOP I; LL, SOP II; and FRL, SOP II are presented. The mean θ_{es} profiles reflect the temperature structure and clearly show the inversion structure. This structure is maintained in the average profile since the inversion height is relatively constant. The θ_{es} maximum at 800 mb marks the inversion top. The inversion base for these average soundings is at approximately 875 mb. The sea surface temperatures from the COADS dataset show little difference between SOP I and SOP II for the LL Region. The temperature, and hence, θ_{es} near the surface are consistent for these two sets of soundings. The soundings from the FRL Region have a lower θ_{es} than the soundings from over the slightly warmer water in Region LL. The profiles of θ_e are similar below the inversion and it is clear that the soundings for the LL Region during SOP I are drier than the equivalent SOP II soundings. Although there is considerable variability in the magnitude of θ_e above the inversion, the shape of the profiles is similar. The QR results in a characteristic θ_e minimum near the inversion with a region of higher θ_e starting at about 750 mb.

A conserved parameter plot (see Betts 1985) of the three sets of soundings in Fig. 8 is presented in Fig. 9. Below the inversion all three mean soundings lie on a well-defined mixing line despite the small variations in temperature and moisture among the mean soundings. The characteristic kink in the mixing line discussed by BA87 is well defined in all three soundings. The points above the inversion appear to fall on a mixing line extending from the surface to near 600 mb.

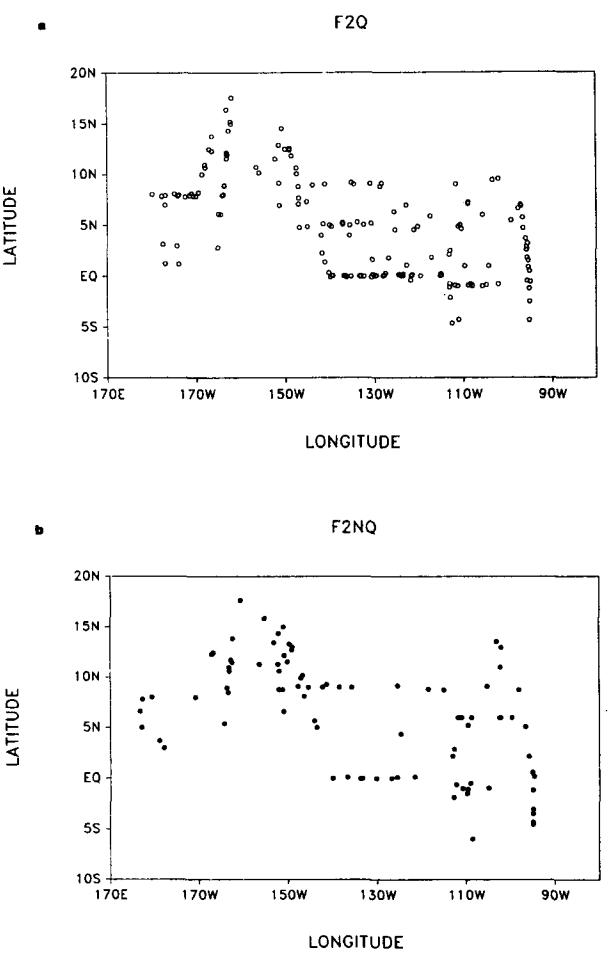

FIG. 7. As Fig. 6, but for SOP II.

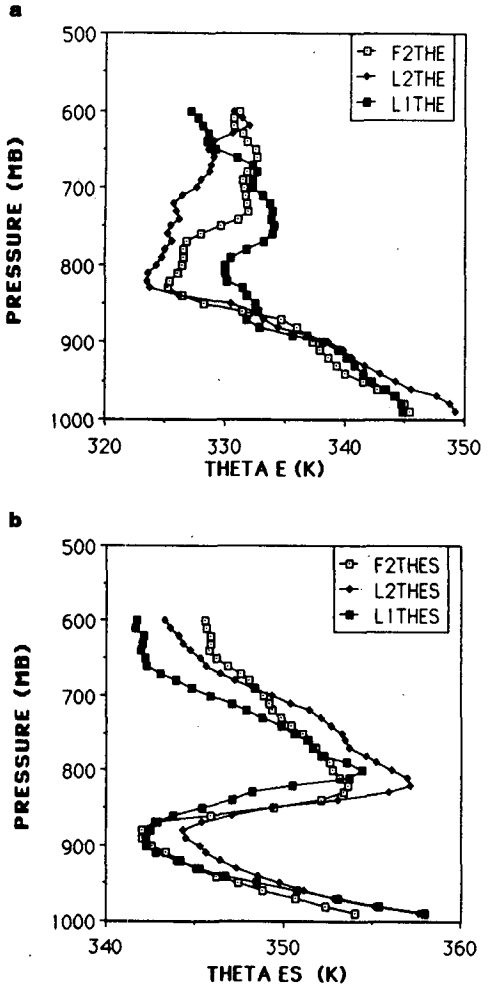

FIG. 8. Profiles (a) θ_e and (b) θ_{es} for soundings with inversion top height from 800–850 mb with QRs for Region LL, SOP I (L1); Region LL, SOP II (L2); and Region FRL, SOP II (F2).

5. Formation of the QR structure

Betts and Albrecht discussed a possible mechanism for the formation of the QR. They proposed that deeper, precipitating cumulus clouds in the vicinity of low-level inversions moisten the levels above the inversion and produce downdrafts that could bring relatively drier air to the top of the inversion. The extensive dataset used in this paper allows us to further evaluate the possible role of deeper, nearby cumulus clouds in forming the QR.

The thermodynamic structure of soundings with the QR were compared with the structure of the corresponding NQR soundings. Since a majority of the soundings had the QR, it was difficult to find regional subsets of soundings that included enough soundings without the QR feature to make useful comparisons. Only subsets that contained at least ten soundings were considered. This restriction gave four regional subsets for the Inversion case and six subsets for the High Theta E case.

For the Inversion cases the comparison is limited to soundings that have similar inversion heights to preserve the structure near the inversion. Although the Inversion subsets with corresponding QR and NQR soundings contained soundings with heights that were not all in the same inversion height range, the subsets from the various regions exhibit similar thermodynamic structures. Profiles of θ_e and θ_{es} for SOP I, Region LL are shown in Fig. 10. The soundings in this subset have inversion tops from 750 mb to 800 mb. This set includes the soundings discussed by BA87. The θ_{es} and θ_e profiles for SOP II, Region FRL are shown in Fig. 11. The differences between the QR and the NQR profiles are similar in both cases, although the θ_e minimum is even more pronounced in the FRL subset than it is in the LL case. The θ_{es} profiles in Figs. 10 and 11 indicate that the boundary layer is slightly warmer in the QR case than it is in the NQR case. For the two subsets shown, θ_e above the minimum at the inversion is higher for the QR soundings than for the NQR soundings. These profiles are similar to those of the two inversion subsets not shown here.

Although the thermodynamic structure for the Inversion cases and the High Theta E cases differ significantly, the thermodynamic structure for the six regional subsets of QR and NQR soundings for the High Theta E classification show little variation. This characteristic structure is illustrated in Fig. 12, which shows θ_e and θ_{es} profiles for High Theta E soundings in Region FRL for QR and NQR soundings. The temperature structure for the QR and the NQR subsets are nearly identical, which results in identical θ_{es} profiles. Both cases are conditionally unstable ($\Delta\theta_{es}/\Delta z \leq 0$) through the boundary layer, which is in sharp contrast to the Inversion case soundings that show a stable layer at the inversion. The High Theta E soundings shown in Fig. 12 do, however, have a layer that is slightly stable from 850 to 750 mb. Some of the soundings in this classification may have weak inversions near this level that give rise to this feature in the mean profiles. Although there is little temperature difference between the QR and NQR soundings, the QR soundings are significantly drier than the NQR soundings. We will show later that the moisture differences for these two cases may reflect differences in the degree of convective mixing.

a. Temperature and moisture differences

The differences between the QR and the NQR structure for the Inversion cases is further illustrated in Figs. 13 and 14 where mixing ratio and potential temperature differences are shown for the two regional subsets of soundings discussed previously. Both subsets show similar differences. The mixing ratio above the inversion is greater for the QR cases than the NQR cases

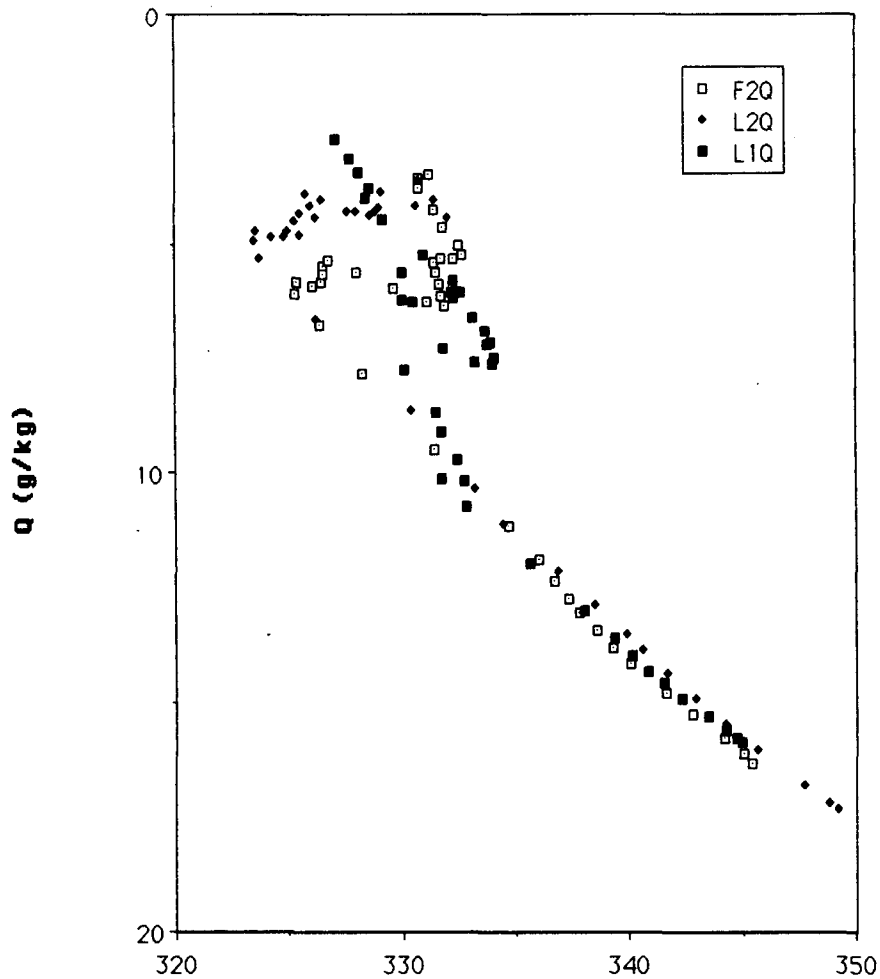

FIG. 9. Conserved parameter (θ_e–q) plot of three sets of soundings shown in Fig. 8.

by about 2 g kg^{-1}. This difference is statistically significant at the 90% ($\alpha = 0.10$) level. At the inversion there is relatively little difference in moisture. Thus an explanation of the QR must include an explanation of the moist layer above the inversion. In addition, the QR soundings are more moist below the inversion than the equivalent NQR soundings. The differences at this level, however, are only significant at the 80% ($\alpha = 0.20$) level. The temperature differences between the QR and NQR soundings shown in Fig. 14 are relatively small above the inversion. Near the surface the QR cases are about 1°C warmer than the NQR cases, although these differences are only significant at the 80% ($\alpha = 0.20$) level.

The QR for Inversion soundings could be formed from NQR soundings if the levels above the top of the inversion are moistened. If this moistening is assumed to be due to a detrainment of cloudy air at this level, the vertical profile of the convective moisture flux and some sense of the magnitude of the fluxes that would be required to give this moistening can be estimated. Following a procedure used by Betts (1976), we estimate the fluxes of total water (vapor and liquid) and liquid water potential temperature that would be needed to give the differences shown in Fig. 13 and 14. Here we choose an arbitrary time interval of one day since this is the approximate time scale for modifications by the large-scale vertical velocity, the other major process that modifies the q structure. Thus the magnitude of the flux divergence can be compared with the time changes of the structure by large-scale processes. If we assume that the perturbation flux is zero at 600 mb, we obtain the flux profiles shown in Fig. 15. The perturbation flux of total water (vapor and liquid, solid symbols) shows the strong moistening above the inversion with slight moistening below the inversion. For the one-day modification assumed here, a flux divergence of approximately 100 W m^{-2} would be required, which is of the same order of magnitude as the surface moisture flux (estimated to be approximately 120 W m^{-2}). If the modification were to occur over a much shorter time period, it would be difficult

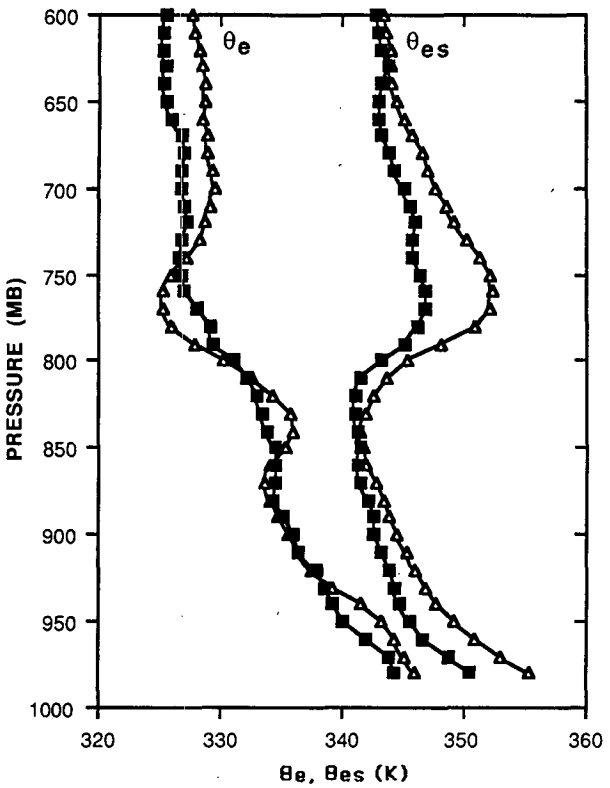

FIG. 10. Mean profiles of θ_e and θ_{es} for the QR (open) cases and NQR (solid) cases for Inversion soundings in SOP I, Region LL, with Inversion top between 750 and 800 mb.

to postulate an appropriate mechanism for the formation of the QR. Although the magnitude of our flux profile is determined by a choice of a one day modification time, the basic shape of the profile is unaffected by this assumption. The flux profile is relatively simple and easily explained by relatively simple convective processes. The flux of liquid water potential temperature is relatively small since the temperature variations are small.

The comparisons shown in Figs. 13 and 14 support the explanation given by BA87. The moist layer above the inversion may result from the detrainment moistening of clouds that may be penetrating the inversion in nearby areas. Detrained cloud air could spread horizontally and modify a relatively large area compared with the area of updraft. Downdrafts, which are cooled by the mixing of dry air into the clouds and further depleted of moisture by precipitation processes, could sink and reach an equilibrium level below the detrained level (or near the inversion top). Although some downdrafts may be sufficiently negatively buoyant to penetrate to the ocean surface, relatively weaker downdrafts would preferentially find equilibrium at the inversion. The weaker downdraft air could spread out at the top of the inversion and influence a relatively large area. Since the downdrafts will spread out at a level where their density is approximately that of the environment, little modification of temperature at this level would be expected, despite changes in the moisture. This modification is similar to downdrafts that penetrate to the surface (e.g. Houze 1977; Zipser 1977; Fitzjarrald and Garstang 1981). Downdrafts that reach the surface, however, may alter the temperature structure since their downward extent is limited by a solid surface and not the local *atmospheric* density stratification. In addition, dry, cool air near the surface would be modified by increased moisture and sensible heat fluxes (Fitzjarrald and Garstang 1981). Just above the inversion the mixing with boundary layer air is inhibited by the inversion and thus the dry air above the inversion may have a relatively long lifetime.

If our hypothesis on the formation of the dry layer is correct, we expect low-level inversions of any strength that are in the vicinity of penetrating downdrafts to act as a depository for dry, downdraft air. The inversion would selectively inhibit downdrafts with (virtual) potential temperatures ranging over that of the temperature difference across the inversion layer. Soundings obtained during GATE following the passage of a deep convective system sometimes showed a moisture reversal above the transition layer inversion that capped

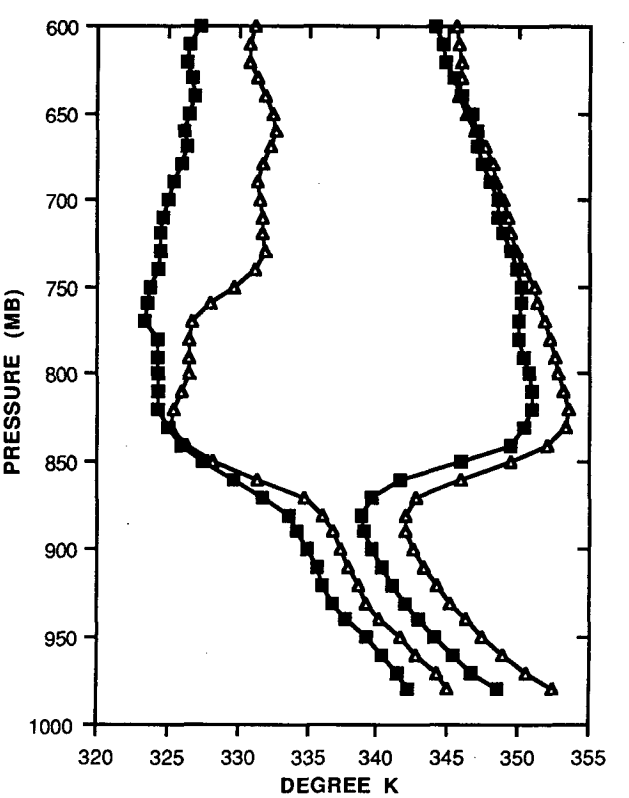

FIG. 11. Mean profiles of θ_e and θ_{es} for the QR (open) cases and NQR (solid) cases for soundings in SOP II, Region FRL, with inversion top between 800 and 850 mb.

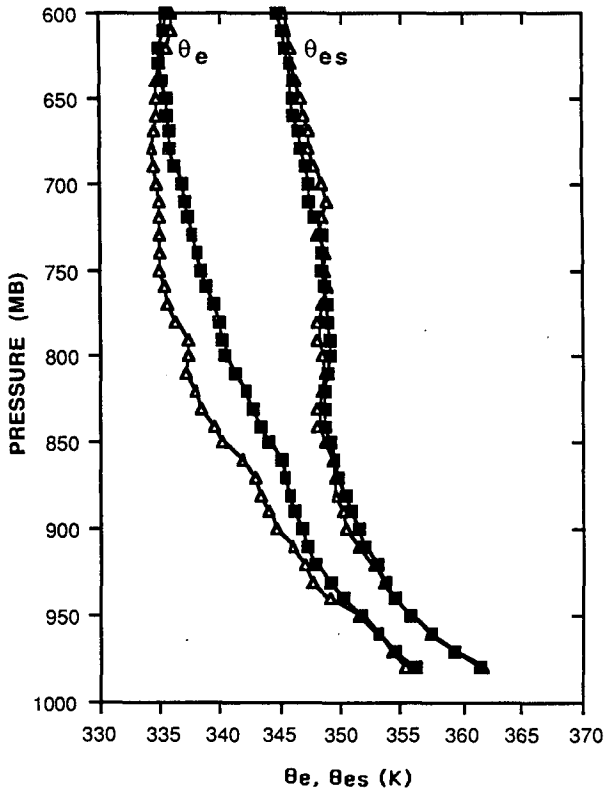

FIG. 12. Mean profiles of θ_e and θ_{es} for the QR (open) cases and NQR (solid) cases for soundings in SOP II, Region FRL, with High Theta E.

the mixed layer (see Fitzjarrald and Garstang 1981, Fig. 6). In addition, Augstein et al. (1974) show a series of soundings obtained at the equator and 30°W from the German ship *Meteor* during 27–29 September 1965. A number of these soundings (see their Fig. 15) show a QR structure above the trade inversion at about 800–850 mb and another reversal above the weaker transition layer inversion at approximately 950 mb.

The differences between the QR and NQR thermodynamic structure discussed previously indicate that clouds originating in the boundary layer may penetrate the QR inversions more easily than the NQR inversions. The temperature and moisture differences shown in Figs. 13 and 14 indicate that QR soundings are warmer at the surface and more moist than the NQR soundings. Since the air above the inversion is about the same for both the QR and the NQR soundings, the QR inversion is slightly weaker than the NQR inversion. Thus, with a higher boundary layer θ_e and a slightly weaker inversion, it is possible that local areas of convection could penetrate the QR inversion more easily than the corresponding NQR inversion.

The warmer and more moist boundary layer observed with the QR soundings may be due to a variety of factors. For example, the QR soundings could have been systematically obtained over a warmer sea surface than the corresponding NQR soundings. Unfortunately, the average SST for the QR and NQR subsets estimated from the smoothed monthly mean SST from the COADS gave differences between the two subsets that were not statistically significant. Furthermore, the regional distribution of the QR shown in Figs. 6 and 7 indicates little regional variation in the occurrence of the QR. Thus, SST may not directly affect the local stability changes associated with the QR. Another possibility is that variations in the trade wind flow may modulate the local stability. Although horizontal variations in temperature and moisture are small by midlatitude standards there are north–south gradients in this area (FA86). Thus, the flow relative to the SST gradients could easily modulate the temperature and moisture structure of the lowest levels. This idea is consistent with the findings of Khalsa (1983) where it was shown that rainfall in the tropics was better correlated with the moisture convergence and the winds than with the local SST. The typical trade flow stabilizes the boundary layer by cold and dry advection. If, however, this trade flow is replaced by a flow that brings air from regions of similar or warmer SST, the boundary layer can be destabilized relative to the trade flow. Unfortunately our dataset is inadequate to test this idea.

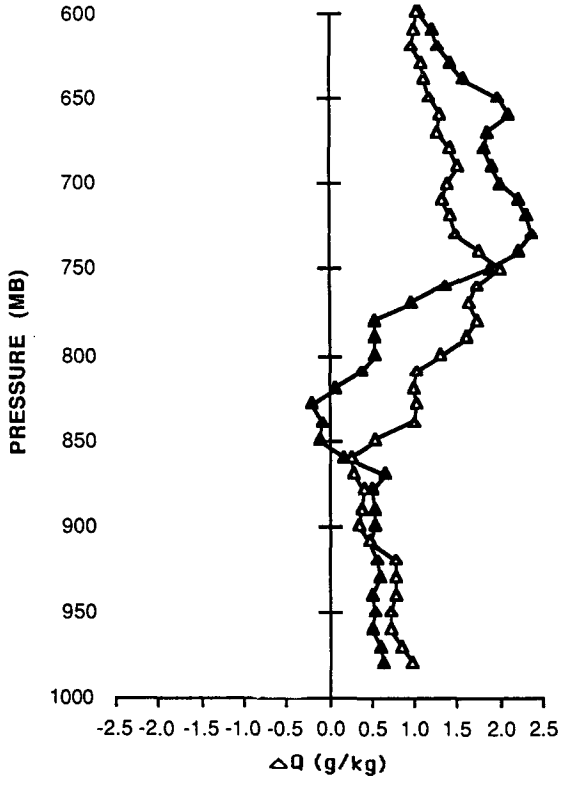

FIG. 13. Mean difference profiles (NQR case subtracted from the QR case) of mixing ratio for the Inversion top height 800–850 mb subsets in SOP II, Regions RL (solid) and FRL (open).

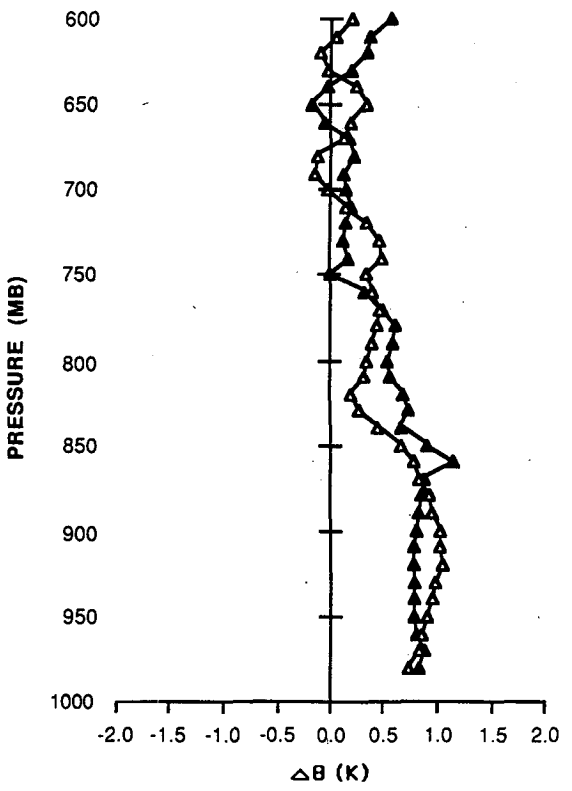

FIG. 14. Mean difference profiles (NQR case subtracted from the QR case) of potential temperature for the Inversion top height 800–850 mb subsets in SOP II, Regions RL (solid) and FRL (open).

We did calculate the meridional winds at 950 mb for the QR and the NQR subsets. Unfortunately, some of the soundings in each subset are north of the convergence zone and others are south of it. Thus the meridional wind by itself is an inadequate parameter to consider for the effect of advection on the stability. If we attempt to further subdivide the soundings, we end up with sample sizes that are too small for meaningful comparisons. Clearly, the effects of SST variations and the modulation of local stability by variations in the trades as a destabilization mechanism needs further study.

It is also possible that radiative effects could play a role in the formation of the QR. For example, the strong longwave cooling at the top of clouds results in a relative destabilization of the boundary layer at night. The soundings were examined to see if there was a diurnal variation in the occurrence of the QR. The soundings were classified into four 2-hour periods from 0600 to 1400 LST. No significant variation in the occurrence of the QR was observed as a function of time. Unfortunately there were insufficient soundings after 1400 to fully evaluate the diurnal characteristics of the boundary layer and inversion layer structure.

b. Conserved parameter analysis

Conserved parameter analyses have a long history of use in interpreting and modeling convective structure and transports. Rossby (1932) suggested the use of θ_e and θ_{es} plots to analyze air mass structure. Paluch (1979) studied entrainment in cumulus clouds using a conserved parameter analysis. Riehl (1954, 1979), and more recently BA87, used conserved parameter plots to study the structure of the tropical atmosphere. The use of conserved parameters simplifies the consideration of phase changes and allows for representations that can be related to physical processes (Betts 1985).

BA87 used q–θ_e plots to graphically illustrate how radiation, precipitation, and mixing processes maintain the characteristic structure of the convective boundary layer and to support their explanation of the QR. We compare the QR and NQR sounding using q–θ_e plots in an attempt to further support and evaluate the role of convective overturning in explaining the formation of the QR.

The q–θ_e profile for the Inversion subsets obtained in the FRL region is shown in Fig. 16. The profile for

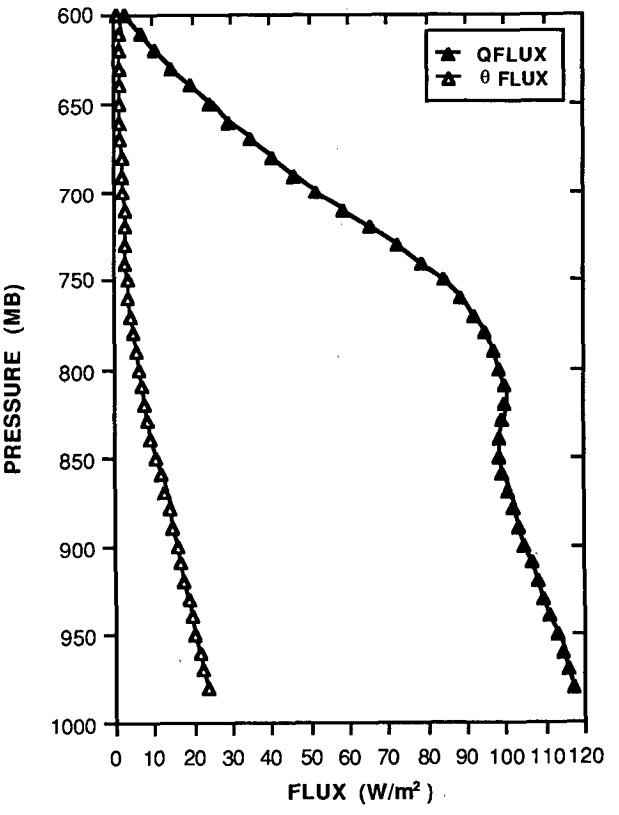

FIG. 15. Vertical perturbation flux of total moisture $[F(q_t)]$ (solid) and liquid water potential temperature $[F(O_L)]$ (open) in W m^{-2} for the subset SOP II, Region FRL, Inversion top height 800–850 mb. Calculated for a 1 day time interval.

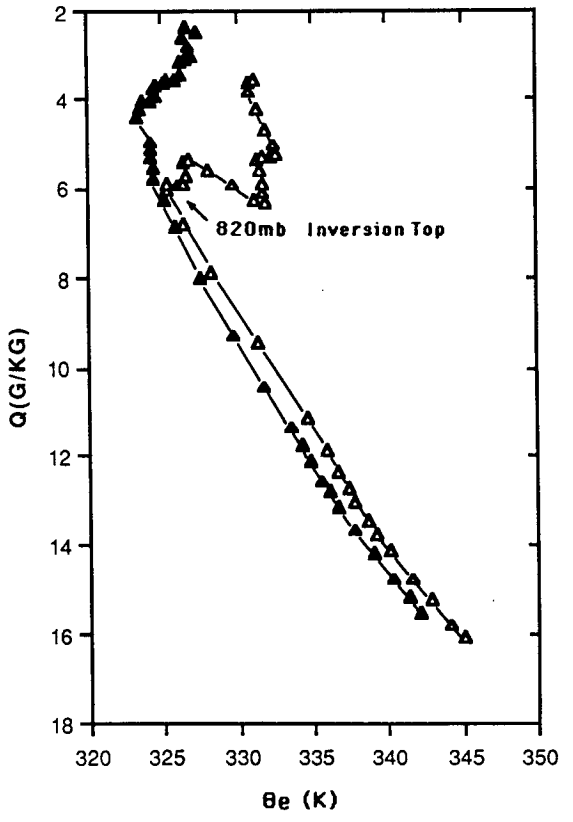

FIG. 16. Mean q–θ_e plot for SOP II, Region FRL, Inversion top between 800–850 mb soundings for QR (open) and NQR (solid).

the QR is denoted by open symbols and the NQR is denoted by solid symbols. The kink structure discussed in BA87 is clearly illustrated, as is the moist layer above the inversion for the QR case. The slope of the mixing line below the inversion is approximately the same for both the QR and the NQR case. The kink in the mixing line structure marks the top of the layer that is thermodynamically coupled to the surface.

The q–θ_e plot for the High Theta E soundings is shown in Fig. 17. The points for the NQR profile fall on a single mixing line. The QR profile, however, has two separate mixing lines with the lower mixing line separated from the upper by a kink structure similar to that observed in the Inversion QR case. A kink structure was observed in five of the six High Theta E subsets. In four of the five subsets with the kink, the kink occurred at 750 mb. The points above this break lie on a mixing line that extends from the surface values to the free atmosphere. These High Theta E soundings clearly have a mixing line structure that differs significantly from the Inversion soundings (Fig. 18).

In contrast, the mixing line structure obtained for the NQR soundings from different geographical regions and for different times of the year showed a remarkably similar mixing line structure (Fig. 9). These results suggest that the classification scheme used in this study provides a meaningful separation of the data and that we can view the mean soundings as representing characteristic structures over a broad region of the tropical Pacific. Although there are large differences between the mixing lines for the High θ_e and the Inversion soundings, the QR High Theta E mixing line structure below the kink has characteristics that are similar to that of the Inversion soundings. In this case there may be deep convection in the region, but the mixing in the low levels has not completely removed the QR. The Inversion QR soundings have a structure above the kink that is very similar to the structure of the High Theta E soundings. The points above the QR lie on a mixing line extending from the surface to the free atmosphere. This structure would be consistent with the detrainment of clouds originating from the boundary layer.

The mixing lines shown in Fig. 18 illustrate the various convective states that exist in all regions. For the NQR Inversion soundings we speculate that few cumulus elements are penetrating the low-level inversion. For the unstable QR Inversion soundings, convective elements in nearby regions may be penetrating the in-

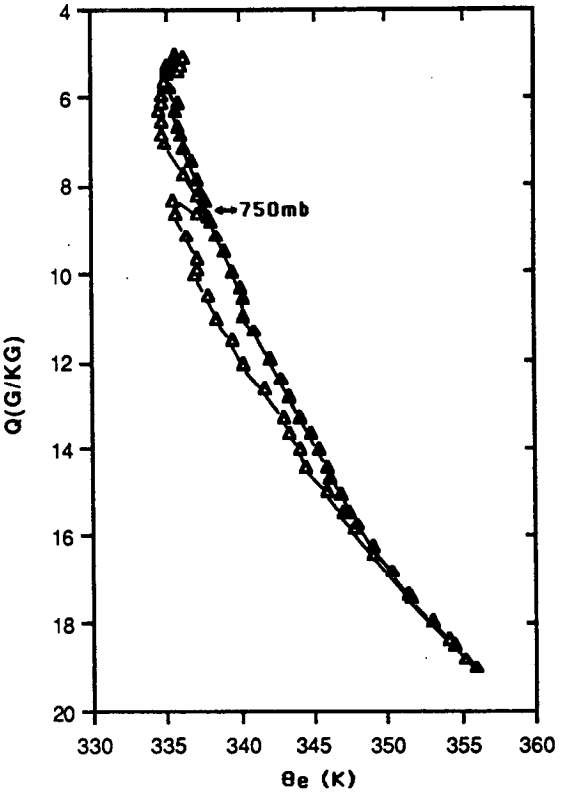

FIG. 17. Mean q–θ_e plot for SOP II, Region FRL, High Theta E soundings for QR (open) and NQR (solid).

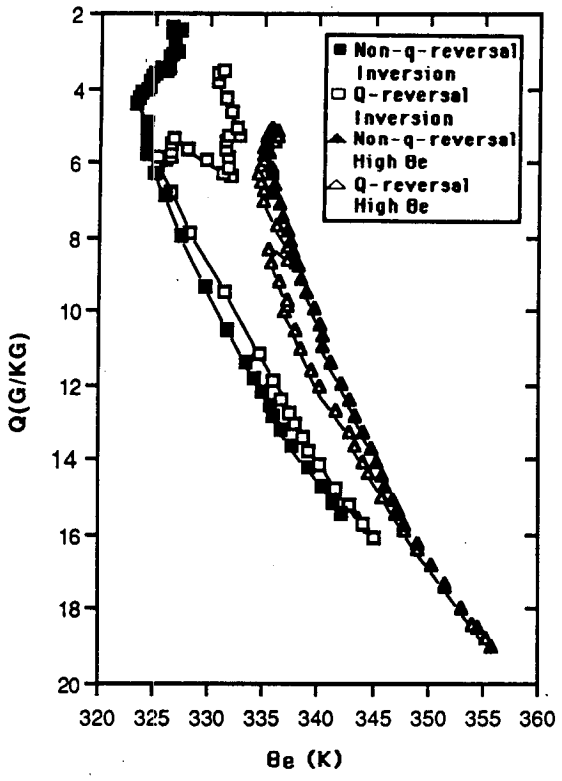

FIG. 18. Mean q–θ_e plots for the QR and NQR cases for the Inversion and High Theta E subsets of Region FRL, SOP II.

version and giving rise to the QR structure as discussed previously. In the unstable QR High Theta E cases we expect that there may be deep convection but that the mixing is incomplete and the kink remains from a previous stable layer or that there are enough soundings with relatively weak inversions to give a QR. In the NQR High Theta E soundings the mixing between the surface and the free atmosphere is sufficient to remove any QR or any stable layers that might produce a QR.

6. Conclusions

Approximately 1200 soundings obtained over the tropical Pacific during FGGE were used to study the structure of the boundary layer over a broad region of the Pacific for January, February, May and June of 1979. The soundings included in this analysis were obtained between 15°N and 5°S and from 90°W to 170°E. These soundings were classified on the basis of the low-level stability. Over 50% of these soundings were found to have a low-level inversion of sufficient strength to inhibit deep convection. Approximately 10% of the soundings were sufficiently cool and dry in the boundary layer to suppress both shallow and deep convection. The remaining soundings were sufficiently unstable to support convection to at least 600 mb. Low-level inversions apparently play a critical role in regulating convection over a broad region of the tropics, which is in agreement with the more limited studies of Ramage et al. (1981) and FA86.

The low-level inversions over the equatorial Pacific were found to have an average inversion top at 800 mb and a base at 850 mb. There was little latitudinal or longitudinal variation in the average height of the inversion, which is again consistent with the findings of Ramage et al. (1981) and FA86. Thus the commonly accepted idea that the height of the trade inversion increases equatorward (Riehl et al. 1951), does not appear to apply between 15°N and the equator over the central and eastern equatorial Pacific. The relatively low inversions may be due to increased subsidence in the region of deeper convection. Thus, the frequency of occurrence of low-level inversions decreases between 15°N and the equator but the mean height of the inversions is relatively constant. It is also possible that even relatively shallow clouds may precipitate and stabilize the boundary layer and thus limit the depth of the convective boundary layer.

About 70% of the soundings with inversions have a reversal in the mixing ratio above the inversion. This reversal (the QR) appears as a relatively dry layer above the inversion that is capped by a relatively moist layer. No regional or temporal variations in the occurrence of the QR were observed. A detailed comparison of the thermodynamic structure for mean soundings with and without the QR show little variation in the mixing ratio at the level where the relative dry layer occurs. Above this layer the QR soundings are more moist by about 2 g kg^{-1} than the corresponding NQR soundings.

In BA87 it was postulated that the QR could be formed by nearby convection that is penetrating to levels above the inversion, moistening the layer above the inversion by detrainment, and forming downdrafts that spread out at the top of the inversion. Our analyses support this idea. The soundings with the QR were found to be slightly more unstable than the corresponding soundings without the QR. The moistening above the dry layer could be accomplished in a period of a day or less by a moisture flux of the same magnitude as the surface moisture flux. A conserved parameter analysis shows that the moist layer above the inversion lies on a mixing line that extends from the surface to approximately 600 mb. There is little difference in the temperature structure above the inversion between the QR and the NQR soundings. This is expected since downdrafts would spread out at a level where the density is similar to that of the downdraft air. Thus, unlike downdraft air that spreads out over a physical surface, the downdrafts spreading out at the top of the inversion would result in relatively little modification of the temperature structure. Futhermore, unlike the strong modification of downdraft air at the surface due to enhanced moisture fluxes, there is no

similar feedback to efficiently eliminate or modify the dry layer just above the inversion top.

We postulate that inversions at any level may serve as a depository for relatively dry downdraft air that impinges on the inversion. Observations obtained during GATE (Fitzjarrald and Garstang 1981) and from the equatorial Pacific in 1965 (Augstein et al. 1974) indicate a relatively dry layer above the transition layer inversion near cloud base.

The QR appears to be a ubiquitous feature of relatively stable boundary layers over the tropical Pacific and has important implications for boundary layer and large-scale models and our general understanding of air–sea interactions over a broad region of the Pacific. When parameterizing boundary layer structures in a large-scale model it is generally assumed that the structure above the boundary layer is explicitly resolved by the model. If this structure is maintained by subgrid-scale processes, then those processes would have to be parameterized. Clearly further study is needed to fully understand the QR structure and its implications.

Acknowledgments. Dr. Paul Julian kindly supplied the dropwindsonde data and Mr. Scott Woodruff supplied the COADS sea-surface temperatures used in this study. We express our gratitude to Miss Elizabeth Gherlone for her assistance with the preparation of this manuscript. This research was supported jointly by the National Science Foundation and the National Oceanic and Atmospheric Administration under Grants ATM 86-11224 and ATM 83-10434, and the U.S. Navy under Grant N000014-86-K-06880.

REFERENCES

Albrecht, B. A., A. K. Betts, W. H. Schubert and S. K. Cox, 1979: A model of the thermodynamic structure of the trade-wind boundary layer. Part I: Theoretical formulation and sensitivity tests. *J. Atmos. Sci.*, **36**, 73–89.

Augstein, E., H. Riehl, F. Ostapoff and V. Wagner, 1973: Mass and energy transports in an undisturbed Atlantic trade-wind flow. *Mon. Wea. Rev.*, **101**, 101–111.

——, H. Schmidt and F. Ostapoff, 1974: The vertical structure of the atmospheric planetary boundary layer in undisturbed trade winds over the Atlantic Ocean. *Bound.-Layer Meteor.*, **6**, 129–150.

Betts, A. K., 1973: Non-precipitating cumulus convection and its parameterization. *Quart. J. Roy. Meteor. Soc.*, **99**, 178–196.

——, 1974: Thermodynamic classification of tropical convective soundings. *Mon. Wea. Rev.*, **102**, 760–764.

——, 1976: The thermodynamic transformation of the tropical subcloud layer by precipitation downdrafts. *J. Atmos. Sci.*, **33**, 1008–1020.

——, 1985: Mixing line analysis of clouds and cloudy boundary layers. *J. Atmos. Sci.*, **42**, 2751–2763.

——, and B. A. Albrecht, 1987: Conserved variable analysis of the convective boundary layer thermodynamic structure over the tropical oceans. *J. Atmos. Sci.*, **44**, 83–99.

Firestone, J. K., and B. A. Albrecht, 1986: The structure of the atmospheric boundary layer in the central equatorial Pacific during January and February of FGGE. *Mon. Wea. Rev.*, **114**, 2219–2231.

Fitzjarrald, D. R., and M. Garstang, 1981: Vertical structure of the tropical boundary layer. *Mon. Wea. Rev.*, **108**, 1512–1526.

Fleming, R. J., T. M. Kaneshige and W. E. McGovern, 1979a: The Global Weather Experiment. Part I: The observational phase through the first Special Observing Period. *Bull. Amer. Meteor. Soc.*, **55**, 649–659.

——, ——, —— and T. E. Bryan, 1979b: The Global Weather Experiment. Part II: The second Special Observing Period. *Bull. Amer. Meteor. Soc.*, **60**, 1316–1322.

Holland, J. S., and B. M. Rasmusson, 1973: Measurements of the atmospheric mass, energy, and momentum budgets over a 500 kilometer square of tropical ocean. *Mon. Wea. Rev.*, **101**, 44–55.

Houze, R. A., Jr., 1977: Structure and dynamics of a tropical squall line system observed during GATE. *Mon. Wea. Rev.*, **105**, 1540–1567.

Julian, P. R., 1982: The aircraft dropwindsonde system in the Global Weather Experiment. *Bull. Amer. Meteor. Soc.*, **63**, 619–627.

Khalsa, S. J. S., 1983: The role of sea surface temperature in large-scale air–sea interaction. *Mon. Wea. Rev.*, **111**, 954–966.

LeMone, M. A., and W. T. Pennell, 1976: The relationship of trade wind cumulus distribution to subcloud layer fluxes and structure. *Mon Wea. Rev.*, **104**, 524–539.

Lilly, D. K., 1968: Models of cloud-topped mixed layers under a strong inversion. *Quart. J. Roy. Meteor. Soc.*, **94**, 874–884.

Nicholls, S., and M. A. LeMone, 1980: The fair weather boundary layer in GATE: The relationship of subcloud fluxes and structure to the distribution and enhancement of cumulus clouds. *J. Atmos. Sci.*, **37**, 2051–2067.

Paluch, I. R., 1979: The entrainment mechanism in Colorado cumuli. *J. Atmos. Sci.*, **36**, 2467–2478.

Ramage, C. S., S. J. S. Khalsa, and B. N. Meisner, 1981: The central Pacific near-equatorial convergence zone. *J. Geophys. Res.*, **86**, 6580–6598.

Reed, R. J., and E. E. Recker, 1971: Structure and properties of synoptic-scale wave disturbances in the equatorial western Pacific. *J. Atmos. Sci.*, **28**, 1117–1133.

Riehl, H., 1954: *Tropical Meteorology*, McGraw Hill, 392 pp.

——, 1979: *Climate and Weather in the Tropics*, Academic Press, 611 pp.

——, T. C. Yeh, J. S. Malkus and N. E. LaSeur, 1951: The northeast trade of the Pacific Ocean. *Quart. J. Roy. Meteor. Soc.*, **77**, 598–626.

Rossby, C. G., 1932: Thermodynamics applied to air mass analysis. Meteor. Pap. Vol. 1, Massachusetts Institute of Technology, 02139. pp. 7–24.

Scribner, O., and J. Smalley, 1981: Aircraft Dropwindsonde Program. U. S. FGGE Project Office: "The Global Weather Experiment-Final Report of U. S. Operations." U. S. FGGE Project Office, NOAA, Rockville, Maryland, 20852, 214 pp.

Stull, R. B., 1988: *An Introduction to Boundary Layer Meteorology*, Kluwer Academic Publishers, 666 pp.

Tiernan, E., 1981: Dropwindsonde Operations, Part 1-The Pacific. U. S. FGGE Project Office: "The Global Weather Experiment-Final Report of U. S. Operations." U. S. FGGE Project Office, NOAA, Rockville, Maryland, 20852, 214 pp.

Yanai, M., S. Esbensen, and J. Chu, 1973: Determination of bulk properties of tropical cloud clusters from large-scale heat and moisture budgets. *J. Atmos. Sci.*, **30**, 611–627.

Zipser, E. J., 1977: Mesoscale and convective-scale downdrafts as distinct components of squall-line circulations. *Mon. Wea. Rev.*, **105**, 1568–1589.